Letter

# Hubble constant in the axi-Higgs universe

Leo W. H. Fung,[1,*] Lingfeng Li,[1,†] Tao Liu,[1,‡] Hoang Nhan Luu,[1,§] Yu-Cheng Qiu,[1,‖] and S.-H. Henry Tye[1,2,¶]

[1]*Department of Physics and Jockey Club Institute for Advanced Study, The Hong Kong University of Science and Technology, Hong Kong SAR, China*

[2]*Department of Physics, Cornell University, Ithaca, New York 14853, USA*

(Received 13 May 2021; revised 29 March 2022; accepted 2 March 2023; published 22 June 2023)

The Λ-cold-dark-matter (ΛCDM) model provides an excellent fit to the cosmic microwave background (CMB) data. However, a statistically significant tension emerges when its determination of the Hubble constant $H_0$ is compared to the local distance-redshift measurements. The axi-Higgs model, which couples an ultralight axion to the Higgs field, offers a specific variation of the ΛCDM model. It relaxes the $H_0$ tension as well as explains the $^7$Li puzzle in big bang nucleosynthesis, the clustering $S_8$ tension with the weak-lensing (WL) data, and the observed isotropic cosmic birefringence in CMB. In this Letter, we demonstrate how the $H_0$ and $S_8$ tensions can be relaxed simultaneously, by correlating the axion impacts on the early and late universe. In a benchmark scenario ($m = 2 \times 10^{-30}$ eV) selected for upcoming experimental tests, the analysis combining the CMB+BAO (baryon acoustic oscillation)+WL+SN data yields $H_0 = 69.9 \pm 1.5$ km/s/Mpc and $S_8 = 0.8045 \pm 0.0096$. Combining this [excluding the SN (supernovae) part] with the local distance-redshift measurements yields $H_0 = 72.42 \pm 0.76$ km/s/Mpc, while $S_8$ is slightly more suppressed.

DOI: 10.1103/PhysRevResearch.5.L022059

*Introduction*. One of the greatest successes in cosmology is the precise measurements of cosmic microwave background (CMB) which support the inflationary-universe paradigm combined with the Λ-cold-dark-matter (ΛCDM) model. However, as data improve, a significant discrepancy emerges between its Hubble constant $H_0 = 67.36 \pm 0.54$ km/s/Mpc determined by Planck 2018 (P18) [1], and $H_0 = 73.3 \pm 0.8$ km/s/Mpc obtained from the local distance-redshift (DR) measurements (see Ref. [2] and also Refs. [3,4] and references therein). At the same time, the ΛCDM/P18 data fitting gives the clustering $S_8 = 0.832 \pm 0.013$ [1], while the recent weak-lensing (WL) data of KiDS-1000 and DES yield $S_8 = 0.766^{+0.020}_{-0.014}$ [5] and $0.773^{+0.026}_{-0.020}$ [6], respectively.

The axi-Higgs model recently proposed [7] suggests a potential solution to the $H_0$ tension by coupling ultralight axions to the Higgs field. This model can further explain the $^7$Li puzzle in big bang nucleosynthesis (BBN) [by shifting the Higgs vacuum expectation value (VEV) [8–18]], as well as the CMB $S_8$ tension with the WL data and the observed isotropic cosmic birefringence (ICB) in CMB [19]. In this Letter, we will demonstrate how this model resolves the $H_0$ and $S_8$ tensions simultaneously, by correlating axion impacts in the early and late universe.

Keeping all parameters in the standard model of particle physics unchanged, the axi-Higgs model with a single axionlike particle $a$ and the electroweak Higgs doublet $\phi$ is given by

$$V(a, \phi, \phi^\dagger) = m^2 a^2/2 + \left|m_s^2 F(a) - \kappa \phi^\dagger \phi\right|^2, \tag{1}$$

$$F(a) = (1 + \delta v)^2 = 1 + C a^2 / M_{\rm Pl}^2, \tag{2}$$

where the axion mass $m$ is $\sim 10^{-30}$–$10^{-29}$ eV [7]; $m_s$ and $\kappa$ are fixed by the Higgs VEV today $v_0 = 246$ GeV and the Higgs mass $m_\phi = 125$ GeV; $\delta v = \Delta v / v_0 = (v - v_0)/v_0$ is the fractional shift of $v$ from $v_0$; $M_{\rm Pl} = 2.4 \times 10^{18}$ GeV is the reduced Planck mass.

The perfect square form of $V(a, \phi, \phi^\dagger)$ here is crucial. It suppresses the impact of the Higgs evolution, such that the axion evolves as if it is free [7]. In this context, the axion (1) lifts $v$ (and hence electron mass $m_e$ [20]) in the early universe (while keeping the Higgs energy density unshifted [7]) and relaxes it to today's value in the late universe, (2) contributes to dark matter (DM) density in the later universe and impacts the comoving diameter distance, (3) explains the ICB data with its Chern-Simons coupling to photons, (4) with its superlong de Broglie wavelength, dampens the clustering amplitude, and (5) provides observable tests via atomic clock and quasar spectral measurements.

Concretely, the axion field stays in a misaligned initial state $a_{\rm ini}$ until the Hubble parameter $H(z)$ drops to $\sim m$. Then $a$ rolls down along the potential, and deposits its vacuum energy into DM. This occurs at the redshift $z_a \sim 1000$–$100$, and determines today's relic abundance $\omega_a$. Since $z_{\rm BBN} \sim 10^9$ at BBN

*whfungad@connect.ust.hk
†iaslfli@ust.hk
‡taoliu@ust.hk
§hnluu@connect.ust.hk
‖yqiuai@connect.ust.hk
¶sht5@cornell.edu

*Published by the American Physical Society under the terms of the Creative Commons Attribution 4.0 International license. Further distribution of this work must maintain attribution to the author(s) and the published article's title, journal citation, and DOI.*

TABLE I. Marginalized parameter values in the ΛCDM model and the axi-Higgs model with $N_Y$ is the number of observables and $N_X$ is the number of model parameters. The upper bounds of $\omega_a$ are shown at 95% confidence level.

| | ΛCDM | Axi-Higgs | ΛCDM | Axi-Higgs |
|---|---|---|---|---|
| | (CMB+BAO+WL+SN) | | (CMB+BAO+WL+DR) | |
| $\omega_b$ | $0.02251 \pm 0.00013$ | $0.02272 \pm 0.00020$ | $0.02267 \pm 0.00013$ | $0.02299 \pm 0.00014$ |
| $\omega_c$ | $0.11801 \pm 0.00081$ | $0.1205 \pm 0.0019$ | $0.11657 \pm 0.00077$ | $0.1228 \pm 0.0014$ |
| $H_0$ | $68.24 \pm 0.36$ | $69.9 \pm 1.5$ | $68.96 \pm 0.34$ | $72.42 \pm 0.76$ |
| $v_{\rm ini}/v_0$ | 1 | $1.0123 \pm 0.0086$ | 1 | $1.0254 \pm 0.0050$ |
| $1000\omega_a$ | 0 | $<1.25$ (95%) | 0 | $<1.32$ (95%) |
| $\omega_\Lambda$ | $0.3244 \pm 0.0056$ | $0.345 \pm 0.020$ | $0.3356 \pm 0.0053$ | $0.377 \pm 0.010$ |
| $\omega_m$ | $0.14116 \pm 0.00078$ | $0.1444 \pm 0.0022$ | $0.13988 \pm 0.00075$ | $0.1470 \pm 0.0017$ |
| $S_8$ | $0.8084 \pm 0.0093$ | $0.8045 \pm 0.0096$ | $0.7902 \pm 0.0088$ | $0.7970 \pm 0.0088$ |
| $100\theta_*$ | $1.04129 \pm 0.00029$ | $1.04115 \pm 0.00030$ | $1.04154 \pm 0.00028$ | $1.04107 \pm 0.00030$ |
| $N_Y - N_X$ | 19−3 | 19−5 | 21−3 | 21−5 |

while $z_* \sim 1100$ at recombination, $a_{\rm ini}$ yields $\delta v_{\rm ini} = \delta v_{\rm BBN} = \delta v_{\rm rec}$ throughout the BBN-recombination epoch. Replacing the coefficient $C$ and $a_{\rm ini}$ by $\delta v_{\rm ini}$ and $\omega_a$ ($C \simeq 0.12\delta v_{\rm ini}/\omega_a$), we have five parameters to determine: the baryon density $\omega_b$, the DM density $\omega_c$ (excluding the $\omega_a$ contribution), $h = H_0/100$ km/s/Mpc, $\delta v_{\rm ini}$, and $\omega_a$, with

$$h^2 = \sum \omega_i = \omega_b + \omega_c + \omega_a + \omega_\Lambda. \tag{3}$$

Considering that the share of $\omega_a$ is tiny and its effects on standard cosmological parameters are typically of percent level, we will apply a leading-order perturbative approach (LPA) [7] in this study. While it is well known that establishing a (semi)analytical relation between the Hubble constant and model parameters would be important for revealing the underlying mechanism to address the Hubble tension (see, e.g., Refs. [21,22]), a systematic method for achieving this goal has been missing. The LPA strongly responds to this need, allowing us to clearly see how a cosmological model such as "axi-Higgs" interplays with the observation data, with relatively small computational effort.

The effects of varying the other cosmological parameters are subleading. So we simply fix them to the default/best-fit values of ΛCDM/P18 [1]. These parameters include the density $\omega_\nu$ for two massless neutrinos and one light one ($m_\nu = 0.06$ eV), $A_s = 2.100\,55 \times 10^{-9}$ and $n_s = 0.966\,05$ of the initial curvature spectrum, and the reionization optical depth $\tau_{\rm re} = 0.054\,31$. Notably, for $m \simeq 10^{-30}$–$10^{-29}$ eV, the axion perturbations affect the low-$l$ plateau of the CMB spectra with a level below that of cosmic variance [23–26], while their effects in the high-$l$ region which are characterized by a sub-Jeans scale are essentially suppressed. The axion perturbations thus can be safely neglected in the LPA analysis here. Note that this feature is not shared by the model of early dark energy (EDE) [27,28], where the favored axion is relatively heavy ($m \simeq 10^{-27}$ eV; see, e.g., Refs. [28–30]) and its perturbation effects hence may not be negligible [31] (see Supplemental Material Sec. C for details [32]).

We summarize the main analysis results in Table I with $m = 2 \times 10^{-30}$ eV as an axi-Higgs benchmark. Combining the CMB+BAO (baryon acoustic oscillation)+WL+SN (supernovae) data yields $H_0 = 69.9 \pm 1.5$ km/s/Mpc and $S_8 = 0.8045 \pm 0.0096$. Especially, $\delta v_{\rm ini} = 1.23\%$ agrees well with $\delta v_{\rm BBN} = 1.2\%$ required to solve the $^7$Li puzzle [7]. The DR data further upshift $H_0$ to $72.42 \pm 0.76$ km/s/Mpc with $\delta v_{\rm ini} = 2.54\%$, which is higher than needed by BBN. This tension however can be solved by introducing a second axion [7], conveniently the one ($m \simeq 10^{-22}$ eV) for fuzzy DM [33–35].

*The LPA analysis*. We separate the LPA analysis into the following steps: (1) Determine the set of parameters $\mathbf{X}$ characterizing the relevant model ($\mathbf{X} \equiv \{\omega_b; \omega_c; h; v_{\rm ini}; \omega_a\}$ for the axi-Higgs model) and a collection of compressed observables $\mathbf{Y}$ representing the data, where $N_Y \geqslant N_X$; (2) define a reference point (here we choose the best fit in the ΛCDM/P18 scenario [1] as the reference point, i.e., $\mathbf{X}_{\rm ref} = \{0.022\,38; 0.1201; 0.6732; v_0; 0\}$), with the observable reference values $\mathbf{Y}_{\rm ref} = \mathbf{Y}(\mathbf{X}_{\rm ref})$; (3) derive variation equations of these observables with respect to $\mathbf{X}$ at the reference point,

$$\delta Y \equiv d\ln Y = Y_{|b}\delta\omega_b + Y_{|c}\delta\omega_c + Y_{|h}\delta h + Y_{|v_{\rm ini}}\delta v_{\rm ini} + Y_{|a}\omega_a, \tag{4}$$

where $Y_{|X} \equiv \partial \ln Y/\partial \ln X$, with an exception of $Y_{|a} \equiv \partial \ln Y/\partial\omega_a$, and their values are calculated either analytically from their definition or numerically using public Boltzmann codes; and (4) apply a likelihood method to these variation equations, to find out the parameter values favored by the data.

The likelihood function is defined as

$$\mathcal{L} = \frac{1}{\sqrt{(2\pi)^{N_Y}|\mathbf{\Sigma}|}} \exp\left[-\frac{1}{2}(\mathbf{Y}_{\rm o} - \mathbf{Y}_{\rm t})^{\rm T}\mathbf{\Sigma}^{-1}(\mathbf{Y}_{\rm o} - \mathbf{Y}_{\rm t})\right], \tag{5}$$

with $\mathbf{Y}_{\rm t} = \mathbf{Y}_{\rm ref}(1 + \delta\mathbf{Y})$. Here, the subscripts "o" and "t" represent the observation values and model predictions, respectively. $\mathbf{\Sigma}$ is the covariance matrix, given by $\mathbf{\Sigma}_{ij} = \rho_{ij}\sigma_i\sigma_j$, where $\rho_{ij}$ measures the observable correlation with $\rho_{ij} = \rho_{ji}$ and $\rho_{ii} = 1$, and $\sigma_i$ is observation variance. The numerical Markov chain Monte Carlo (MCMC) sampler COBAYA [36] is used to sample the likelihood function for our analysis.

To represent the CMB data, we consider the sound horizon at recombination $l_a$, the Hubble horizon at matter-radiation equality $l_{\rm eq}$, the damping scale at recombination $l_D$ and $S_L$. $l_a$ determines the position of the first acoustic peak and also the peak spacings. $l_{\rm eq}$ sets up the threshold for radiation to dominantly drive gravitational potential, while $l_D$ is the scale below which fluctuations are suppressed by photon-baryon coupling

TABLE II. Representative $Y_{|X}$ values in the axi-Higgs model. The $\Lambda$CDM$(+m_e)$ model shares the values of $Y_{|b,c,h}(+Y_{|v_{\rm ini}})$.

| | $X$ | | | | |
|---|---|---|---|---|---|
| $Y$ | $\omega_b$ | $\omega_c$ | $h$ | $v_{\rm ini}$ | $\omega_a$ |
| $l_a$ | 0.0550 | − 0.1203 | − 0.1934 | 0.6837 | − 2.6364 |
| $l_{\rm eq}$ | 0.0942 | 0.5082 | − 0.1934 | 0.0154 | − 2.6376 |
| $l_D$ | 0.2459 | − 0.0962 | − 0.1934 | 0.4553 | − 2.6315 |
| $S_L$ | − 0.1398 | 0.8484 | − 0.2619 | 0.0788 | − 16.082 |
| $\alpha_\perp(0.698)$ | 0.1466 | 0.0969 | − 0.7175 | | − 0.9852 |
| $\alpha_\parallel(0.698)$ | 0.1256 | − 0.0160 | − 0.4483 | 0.6162 | − 1.9252 |
| $\alpha_V(0.845)$ | 0.1354 | 0.0370 | − 0.5747 | | − 1.4838 |
| $S_8$ | − 0.1007 | 1.0578 | − 0.7658 | 0.0788 | − 14.337 |
| $m_B(1.36)$ | − 0.0018 | − 0.0099 | 0.0237 | 0 | − 0.0829 |

and multipole anisotropic stress. Phenomenologically, $l_{\rm eq}$ and $l_D$ determine the relative peak heights while $l_{\rm eq}$ also determines the modulation between the even and odd peaks. As pointed out in Refs. [37–39], the CMB temperature spectrum $C_\ell^{\rm TT}$ can be effectively characterized by these scale parameters. The CMB polarization spectrum $C_\ell^{\rm EE}$ and cross spectrum $C_\ell^{\rm TE}$ measure similar acoustic features [1] and can couple to these scales also. As for $S_L \equiv \sigma_8\Omega_m^{0.25}$ [40], it encodes the CMB lensing spectrum $C_\ell^{\phi\phi}$ and reflects the CMB constraints on matter fluctuation. Moreover, we include the BAO scale parameters in the direction transverse $[\alpha_\perp(z_{\rm eff})]$ and parallel $[\alpha_\parallel(z_{\rm eff})]$ to the line of sight, respectively, and the isotropic BAO scale parameter $[\alpha_V(z_{\rm eff})]$, the galaxy-clustering amplitude $(S_8)$ from WL, and the supernova luminosity $[m_B(z_{\rm eff})]$ (or the local DR measurements). Conveniently, we denote $\mathbf{Y}_{\rm CMB} = \{l_a, l_{\rm eq}, l_D, S_L\}$, $\mathbf{Y}_{\rm BAO} = \{\alpha_\perp(z_{\rm eff}), \alpha_\parallel(z_{\rm eff}), \alpha_V(z_{\rm eff})\}$, $\mathbf{Y}_{\rm WL} = \{S_8\}$, $\mathbf{Y}_{\rm SN} = \{m_B(z_{\rm eff})\}$, and $\mathbf{Y}_{\rm DR} = \{H_0\}$. The data respectively applied to them include the following:

(1) CMB: P18 (TT,TE,EE + lowE + lensing) data [1];

(2) BAO: low-$z$ surveys 6dF [41], MGS [42], and high-$z$ eBOSS ELG [43] for $\alpha_V$; high-$z$ eBOSS LRG [44], Quasar [45], Lyman-$\alpha$ [46] for $\alpha_\perp$, $\alpha_\parallel$;

(3) WL: DES Y1 [6] and KiDs-1000 [5];

(4) SN: Binned Pantheon samples [47];

(5) DR: SH0ES-19 [48], H0LiCOW [49], MCP [50], CCHP [51], SBF [52], and MIRAS [53].

Combining these data yields a block-diagonal covariance matrix: $\mathbf{\Sigma} = {\rm diag}\{\mathbf{\Sigma}_{\rm CMB}, \mathbf{\Sigma}_{\rm BAO}, \mathbf{\Sigma}_{\rm WL}, \mathbf{\Sigma}_{\rm SN/DR}\}$.

The $Y_{|X}$ values are presented in Table II (see Supplemental Material Secs. A and B [32] for a full list of $\mathbf{Y}$ and $\mathbf{\Sigma}$, and $Y_{|X}$, respectively). The relevant variation equations then can be read out directly, using these $Y_{|X}$ values as the inputs of Eq. (4). For example, we have

$$\begin{aligned}\delta l_{\rm eq} &= 0.0942\delta\omega_b + 0.5082\delta\omega_c - 0.1934\delta h \\ &\quad + 0.0154\delta v_{\rm ini} - 2.6376\omega_a \end{aligned} \tag{6}$$

for $Y = l_{\rm eq}$. Since $l_{\rm eq}$ has been precisely measured, a shift in $h$ has to be compensated for by shifts in the other quantities, to keep $\delta l_{\rm eq} \simeq 0$. Separately, with $S_{8|a} \ll 0$, lowering $S_8$ needs only a small $\omega_a$.

We first test the LPA validation with $\mathbf{Y}_{\rm CMB}$ in the $\Lambda$CDM model. As shown in Fig. 1, the LPA exceptionally reproduces

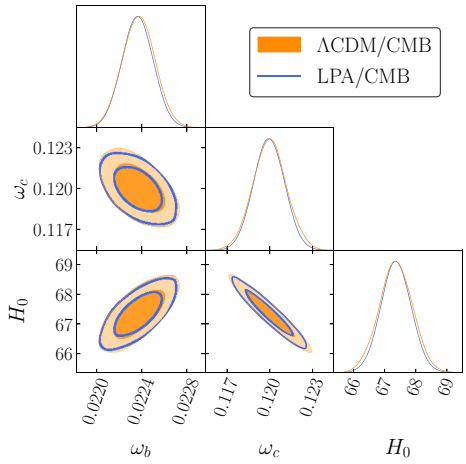


FIG. 1. Comparison of the marginalized contours and posterior distributions of $\Lambda$CDM between the LPA and the P18's [1] analyses.

the marginalized contours of $\omega_b$, $\omega_c$, and $H_0$ and their posterior distributions obtained by P18 [1]. Numerically, the LPA results ($\mathbf{X}_{\rm LPA}$) only differ from the marginalized $\Lambda$CDM/P18 ones ($\mathbf{X}_{\rm P18}$) slightly, for both central values and their uncertainties (see Table III). The LPA is equally successful while being applied to the $\Lambda{\rm CDM} + m_e$ model [54,55], where $\delta v_{\rm ini} = \delta m_e$. This provides an even more crucial test on the LPA validity as this model is characterized by its own parameters. The LPA validity is then expected for the axi-Higgs model (see Supplemental Material Sec. D [32] for details): In terms of cosmological phenomenology, the axi-Higgs model differs from $\Lambda{\rm CDM} + m_e$ mainly in the impacts on the comoving distance to last scattering. Note, for other cosmological models, the LPA validity needs to be further tested.

*$H_0$ and $S_8$ in the axi-Higgs universe*. Despite the sharing of $m_e$ as a free parameter in the recombination epoch, the axi-Higgs model is essentially different from $\Lambda{\rm CDM} + m_e$, due to the impacts of the time-varying axion field. According to Refs. [54,56], an upward shift of $m_e$ will reduce the cross section of Thomson scattering $(\propto m_e^{-2})$ and modify various atomic processes crucial to recombination. It thus increases $z_*$ and decreases the comoving sound horizon and damping scale at $z_*$. The axion evolution here causes a positive shift to $v$ or $m_e$ at $z > z_a$ and then brings it back later to today's value [7]. In contrast, such a mechanism is lacking for $\Lambda{\rm CDM} + m_e$ [54,56]. Moreover, the axion at $z < z_a$ tends to reduce the comoving diameter distance, because of its contribution to $H(z)$. This provides extra flexibility to resolve the impacts of varying $H_0$ on the CMB scale parameters. As to be shown below, a combination of these effects raises $H_0$ to a value higher than what the $\Lambda{\rm CDM} + m_e$ model allows, without breaking our knowledge on today's electron.

Let us start with the Hubble flow of axi-Higgs,

$$\begin{aligned} H(z) = 100\ {\rm km/s/Mpc}[&\omega_r(1+z)^4 + (\omega_c + \omega_b) \\ &\times (1+z)^3 + g(z)\omega_a + \omega_\Lambda]^{\frac{1}{2}}, \end{aligned} \tag{7}$$

where $\omega_r$ is the radiation density, and

$$g(z) = \begin{cases} (1+z)^3, & z \ll z_a < z_*, \\ (1+z_a)^3, & z > z_a. \end{cases} \tag{8}$$

TABLE III. Test of the LPA validity in the ΛCDM model.

| **X** | $\omega_b$ | $\omega_c$ | $h$ | $S_8$ |
|---|---|---|---|---|
| $\mathbf{X}_{\rm P18}$ [1] | $0.02237 \pm 0.00015$ | $0.1200 \pm 0.0012$ | $0.6736 \pm 0.0054$ | $0.832 \pm 0.013$ |
| $\mathbf{X}_{\rm LPA}$ | $0.02237 \pm 0.00014$ | $0.1200 \pm 0.0011$ | $0.6735 \pm 0.0050$ | $0.832 \pm 0.013$ |

The evolution of $\delta H(z) = [H(z) - H_{\rm ref}(z)]/H_{\rm ref}(z)$ and its derivatives with respect to $\omega_{b,c,a,\Lambda}$ then can be derived from this formula. We show both of them in Fig. 2 using the best fit of ΛCDM/P18 as the reference scenario as before. According to this figure, $H(z)$ deviates from its ΛCDM prediction since $z > z_{\rm eq}$, which is sequentially taken over by $\omega_c$, $\omega_a$, and $\omega_\Lambda$. The evolution of $H(z)_{|a}$ can be separated into three stages. In the early time, the axion is dark energy (DE)-like. $H(z)_{|a}$ evolves as $\propto 1/\omega_r(1+z)^4$ for $z > z_{\rm eq}$ and $\propto 1/(\omega_b+\omega_c)(1+z)^3$ after that. So its value is suppressed at high redshift. This lasts until the axion becomes DM-like at $z \sim z_a$. $H(z)_{|a}$ then evolves roughly as a constant $\propto 1/\omega_m$ during $z \sim 100 - 1$, with a wiggling feature developed for its curve due to axion oscillation. In the Λ-dominant epoch ($z < 1$), $H(z)_{|a}$ drops quickly as $z$ goes to zero, as $H(z)_{|a} \propto (1+z)^3/\omega_\Lambda$. Such an evolution pattern of $H(z)_{|a}$, particularly its big value after recombination, results in a universal negative dependence of the CMB and BAO scale parameters on $\omega_a$ (see Table II and Supplemental Material Sec. B [32] for details). Consider $l_{\rm eq} \propto H(z_{\rm eq})D_*$ as an example. $H(z_{\rm eq})$ is determined by the early-time cosmology and hence less influenced by $\omega_a$, while the diameter distance $D_* = \int_0^{z_*} \frac{dz'}{H(z')}$ is closely related to cosmic evolution after recombination, varied as $\sim \int_0^{z_*} \frac{-H(z')_{|a}\omega_a dz'}{H(z')^2}$ with respect to $\omega_a$. So we necessarily have $l_{{\rm eq}|a} < 0$ (as a comparison, we have $l_{{\rm eq}|c} > 0$). Note, both $H(z_{\rm eq})$ and $D_*$ and hence $l_{\rm eq}$ are insensitive to $\delta v_{\rm ini}$.

In ΛCDM, an $H_0$ value from local DR measurements is highly disfavored by the CMB data due to its correlation with $\omega_b$ and $\omega_c$. The Friedman equation for today's universe [see Eq. (3)] indicates that, as $h$ increases, $\omega_i$ tends to increase faster. Being out of phase between these variations breaks the variation equations of the CMB/BAO scale parameters defined by Table II. However, the situation gets changed in the axi-Higgs model. Among these scale parameters, varying $h$ tends to have the largest impact on $l_{\rm eq}$ via $\delta\omega_c$. This impact is largely canceled by the $\omega_a$ contribution. As discussed above [also see Eq. (6)], $\delta l_{\rm eq}$ has an opposite dependence on $\delta\omega_c$ and $\omega_a$. As for the impacts brought in by the requested $\omega_a$ on the other scale parameters, they will be absorbed by a positive $\delta v_{\rm ini}$ which also compensates for the impacts of shifting $h$. Except $l_{\rm eq}$, these parameters demonstrate a positive and comparable dependence on $\delta v_{\rm ini}$, due to the universal impacts of $\delta v$ on the sound horizon at recombination and the end of baryon drag. The interplay of these parameters finally mitigates the $H_0$ tension. Notably, although the effect of varying $m_e$ in the $\Lambda{\rm CDM} + m_e$ model can be encoded as that of $\delta v_{\rm ini}$ here, the absence of $\omega_a$ worsens the fitting of $l_{\rm eq}$ and hence limits the allowed values for $h$ greatly.

We demonstrate the axi-Higgs posterior distributions for the benchmark of $m = 2 \times 10^{-30}$ eV in Fig. 3 (see Supplemental Material Sec. E for the impacts of the axion mass on data fitting, and Sec. F for an overall picture on the axi-Higgs cosmology [32]). Compared to the ΛCDM/CMB [1] and $\Lambda{\rm CDM} + m_e/{\rm CMB} + {\rm BAO}$ [55] analyses, the axi-Higgs/CMB + BAO + WL + SN scenario yields a higher $H_0$ value, accompanied by a downward shift of $S_8$ (due

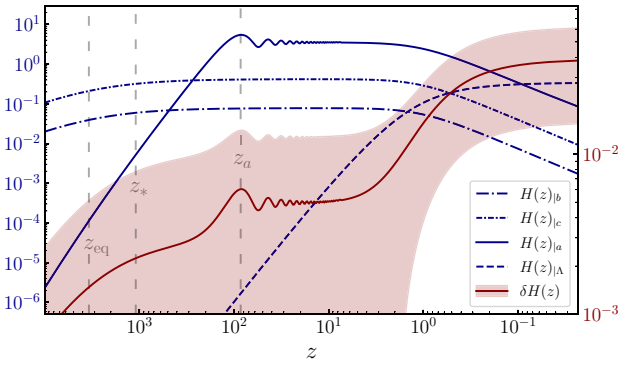


FIG. 2. Evolution of $H(z)_{|b,c,a,\Lambda}$ and $\delta H(z)$ in the axi-Higgs benchmark, with the CMB+BAO+WL+SN data. $z_{\rm eq}$ denotes the redshift at the moment of matter-radiation equality.

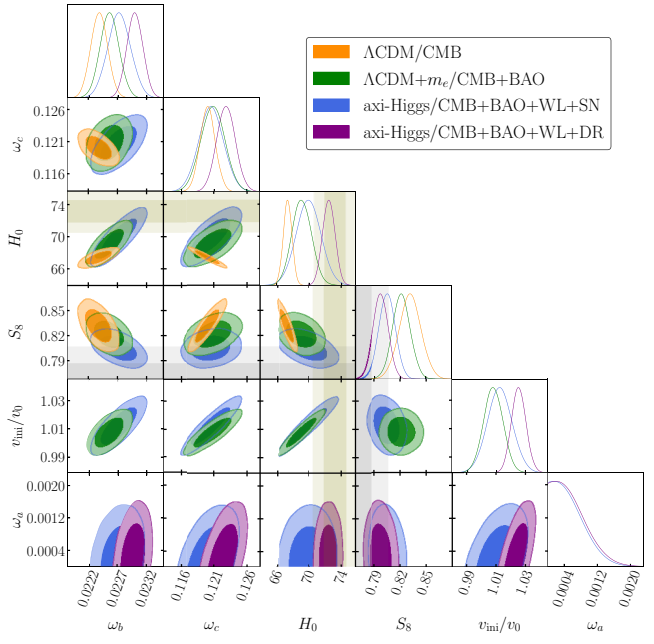


FIG. 3. Posterior distributions of the model parameters in the axi-Higgs benchmark scenario. The shaded olive and gray bands represent the local DR measurement of $H_0$ from the latest SH0ES-20 [57] and the weak-lensing measurement of $S_8$ from KiDS-1000 [5], respectively.

to $S_{8|a} \ll 0$ and $\omega_a > 0$). The blue solid contours overlap with the intersection of the shaded olive and gray bands in the $H_0$-$S_8$ panel. The $H_0$ and $S_8$ tensions are thus simultaneously reduced.

*Summary and remarks*. As a low-energy effective theory motivated by string theory, the axi-Higgs model broadly impacts our understanding of the universe [7]. In this Letter, we have demonstrated how the $H_0$ and $S_8$ tensions get simultaneously relaxed in this model, by correlating the axion impacts on the early and late universe.

In the early universe ($z > z_a$), this axion field behaves as DE. Its main impact is to drive a positive shift in the Higgs VEV. In the late universe ($z < z_a$), this axion field behaves as DM. Its main impacts are to (1) increase the $H(z)$ value during this epoch and hence reduce the comoving diameter distance at $z_*$ and $z_{\rm eff}$, (2) suppress the formation of the structure at a galactic clustering scale and even above, and (3) shift the $v$ (or $m_e$) value in the early universe to today's value $v_0$. Combining the axion impact at $z > z_a$ and item (1) mitigates the Hubble tension, further including item (2) relaxes the $S_8$ tension, and finally including item (3) restores our observation on today's electron.

To conclude, we stress that a full test of this model is at hand, due to the oncoming Atomic Clock and the quasar spectral measurements with the data expected to be collected by, e.g., the Thirty Meter Telescope [58] and James Webb Space Telescope [59]. More details on this can be found in Ref. [7].

*Acknowledgments.* We thank Luke Hart and Jens Chluba for valuable communications. This work is supported partly by the Area of Excellence under the Grant No. AoE/P-404/18 and partly by the General Research Fund under Grant No. 16305219. All grants were issued by the Research Grants Council of Hong Kong SAR.

[1] N. Aghanim, Y. Akrami, M. Ashdown, J. Aumont, C. Baccigalupi, M. Ballardini, A. J. Banday, R. B. Barreiro, N. Bartolo, S. Basak *et al.* (Planck), Planck 2018 results. VI. Cosmological parameters, Astron. Astrophys. **641**, A6 (2020).

[2] L. Verde, T. Treu, and A. G. Riess, Tensions between the early and the late universe, Nat. Astron. **3**, 891 (2019).

[3] L. Knox and M. Millea, Hubble constant hunter's guide, Phys. Rev. D **101**, 043533 (2020).

[4] E. Di Valentino, O. Mena, S. Pan, L. Visinelli, W. Yang, A. Melchiorri, D. F. Mota, A. G. Riess, and J. Silk, In the realm of the Hubble tension—a review of solutions, Class. Quantum Grav. **38**, 153001 (2021).

[5] C. Heymans *et al.*, KiDS-1000 Cosmology: Multi-probe weak gravitational lensing and spectroscopic galaxy clustering constraints, Astron. Astrophys. **646**, A140 (2021).

[6] T. M. C. Abbott *et al.* (DES), Dark Energy Survey year 1 results: Cosmological constraints from galaxy clustering and weak lensing, Phys. Rev. D **98**, 043526 (2018).

[7] L. W. H. Fung, L. Li, T. Liu, H. N. Luu, Y.-C. Qiu, and S. H. H. Tye, Axi-Higgs cosmology, J. Cosmol. Astropart. Phys. **08**, 057 (2021).

[8] J. P. Kneller and G. C. McLaughlin, Big bang nucleosynthesis and $\lambda_{\rm QCD}$, Phys. Rev. D **68**, 103508 (2003).

[9] B. Li and M.-C. Chu, Big bang nucleosynthesis with an evolving radion in the brane world scenario, Phys. Rev. D **73**, 023509 (2006).

[10] A. Coc, N. J. Nunes, K. A. Olive, J.-P. Uzan, and E. Vangioni, Coupled variations of fundamental couplings and primordial nucleosynthesis, Phys. Rev. D **76**, 023511 (2007).

[11] T. Dent, S. Stern, and C. Wetterich, Primordial nucleosynthesis as a probe of fundamental physics parameters, Phys. Rev. D **76**, 063513 (2007).

[12] T. E. Browder, T. Gershon, D. Pirjol, A. Soni, and J. Zupan, New physics at a Super Flavor Factory, Rev. Mod. Phys. **81**, 1887 (2009).

[13] P. F. Bedaque, T. Luu, and L. Platter, Quark mass variation constraints from Big Bang nucleosynthesis, Phys. Rev. C **83**, 045803 (2011).

[14] M.-K. Cheoun, T. Kajino, M. Kusakabe, and G. J. Mathews, Time-dependent quark masses and big bang nucleosynthesis revisited, Phys. Rev. D **84**, 043001 (2011).

[15] J. C. Berengut, E. Epelbaum, V. V. Flambaum, C. Hanhart, U.-G. Meissner, J. Nebreda, and J. R. Pelaez, Varying the light quark mass: impact on the nuclear force and big bang nucleosynthesis, Phys. Rev. D **87**, 085018 (2013).

[16] L. J. Hall, D. Pinner, and J. T. Ruderman, The weak scale from BBN, J. High Energy Phys. 12 (2014) 134.

[17] M. Heffernan, P. Banerjee, and A. Walker-Loud, Quantifying the sensitivity of big bang nucleosynthesis to isospin breaking with input from lattice QCD, arXiv:1706.04991.

[18] K. Mori and M. Kusakabe, Roles of $^7$Be$(n, p)^7$Li resonances in big bang nucleosynthesis with time-dependent quark mass and Li reduction by a heavy quark mass, Phys. Rev. D **99**, 083013 (2019).

[19] Y. Minami and E. Komatsu, New Extraction of the Cosmic Birefringence from the Planck 2018 Polarization Data, Phys. Rev. Lett. **125**, 221301 (2020).

[20] Massive particles couple to the Higgs field usually. But, only electrons are relevant here: The protons receive a contribution to their mass dominantly from strong dynamics, while massive elementary particles except electrons are too heavy to affect recombination significantly.

[21] K. Jedamzik, L. Pogosian, and G.-B. Zhao, Why reducing the cosmic sound horizon alone can not fully resolve the Hubble tension, Commun. Phys. **4**, 123 (2021).

[22] T. Sekiguchi and T. Takahashi, Early recombination as a solution to the $H_0$ tension, Phys. Rev. D **103**, 083507 (2021).

[23] D. J. E. Marsh, Axion cosmology, Phys. Rep. **643**, 1 (2016).

[24] R. Hlozek, D. Grin, D. J. E. Marsh, and P. G. Ferreira, A search for ultralight axions using precision cosmological data, Phys. Rev. D **91**, 103512 (2015).

[25] R. Hlozek, D. J. E. Marsh, and D. Grin, Using the full power of the cosmic microwave background to probe axion dark matter, Mon. Not. R. Astron. Soc. **476**, 3063 (2018).

[26] G. Franco Abellán, Z. Chacko, A. Dev, P. Du, V. Poulin, and Y. Tsai, Improved cosmological constraints on the neutrino mass and lifetime, J. High Energy Phys. 08 (2022) 076.

[27] T. Karwal and M. Kamionkowski, Dark energy at early times, the Hubble parameter, and the string axiverse, Phys. Rev. D **94**, 103523 (2016).

[28] V. Poulin, T. L. Smith, T. Karwal, and M. Kamionkowski, Early Dark Energy Can Resolve the Hubble Tension, Phys. Rev. Lett. **122**, 221301 (2019).

[29] M.-X. Lin, G. Benevento, W. Hu, and M. Raveri, Acoustic dark energy: Potential conversion of the Hubble tension, Phys. Rev. D **100**, 063542 (2019).

[30] P. Agrawal, F.-Y. Cyr-Racine, D. Pinner, and L. Randall, Rock 'n' roll solutions to the Hubble tension, arXiv:1904.01016.

[31] V. Poulin, T. L. Smith, D. Grin, T. Karwal, and M. Kamionkowski, Cosmological implications of ultralight axion-like fields, Phys. Rev. D **98**, 083525 (2018).

[32] See Supplemental Material at http://link.aps.org/supplemental/10.1103/PhysRevResearch.5.L022059 for additional calculations and analyses in support of the results presented in this paper.

[33] W. Hu, R. Barkana, and A. Gruzinov, Fuzzy Cold Dark Matter: The Wave Properties of Ultralight Particles, Phys. Rev. Lett. **85**, 1158 (2000).

[34] H.-Y. Schive, T. Chiueh, and T. Broadhurst, Cosmic structure as the quantum interference of a coherent dark wave, Nat. Phys. **10**, 496 (2014).

[35] L. Hui, J. P. Ostriker, S. Tremaine, and E. Witten, Ultralight scalars as cosmological dark matter, Phys. Rev. D **95**, 043541 (2017).

[36] J. Torrado and A. Lewis, Cobaya: Code for Bayesian analysis of hierarchical physical models, J. Cosmol. Astropart. Phys. **05**, 057 (2021).

[37] W. Hu, N. Sugiyama, and J. Silk, The physics of microwave background anisotropies, Nature (London) **386**, 37 (1997).

[38] W. Hu, M. Fukugita, M. Zaldarriaga, and M. Tegmark, CMB observables and their cosmological implications, Astrophys. J. **549**, 669 (2001).

[39] W. Hu and S. Dodelson, Cosmic microwave background anisotropies, Annu. Rev. Astron. Astrophys. **40**, 171 (2002).

[40] N. Aghanim *et al.* (Planck), Planck 2018 results. VIII. Gravitational lensing, Astron. Astrophys. **641**, A8 (2020).

[41] F. Beutler, C. Blake, M. Colless, D. H. Jones, L. Staveley-Smith, L. Campbell, Q. Parker, W. Saunders, and F. Watson, The 6df Galaxy Survey: Baryon acoustic oscillations and the local Hubble constant, Mon. Not. R. Astron. Soc. **416**, 3017 (2011).

[42] A. J. Ross, L. Samushia, C. Howlett, W. J. Percival, A. Burden, and M. Manera, The clustering of the SDSS DR7 main Galaxy sample – I. A 4 per cent distance measure at $z = 0.15$, Mon. Not. R. Astron. Soc. **449**, 835 (2015).

[43] A. Raichoor *et al.*, The completed SDSS-IV extended baryon oscillation spectroscopic survey: Large-scale structure catalogues and measurement of the isotropic BAO between redshift 0.6 and 1.1 for the Emission line galaxy sample, Mon. Not. R. Astron. Soc. **500**, 3254 (2020).

[44] J. E. Bautista *et al.*, The completed SDSS-IV extended baryon oscillation spectroscopic survey: Measurement of the BAO and growth rate of structure of the luminous red galaxy sample from the anisotropic correlation function between redshifts 0.6 and 1, Mon. Not. R. Astron. Soc. **500**, 736 (2020).

[45] R. Neveux *et al.*, The completed SDSS-IV extended baryon oscillation spectroscopic survey: BAO and RSD measurements from the anisotropic power spectrum of the quasar sample between redshift 0.8 and 2.2, Mon. Not. R. Astron. Soc. **499**, 210 (2020).

[46] H. du Mas des Bourboux *et al.*, The completed SDSS-IV extended baryon oscillation spectroscopic survey: Baryon acoustic oscillations with Ly$\alpha$ forests, Astrophys. J. **901**, 153 (2020).

[47] D. M. Scolnic *et al.*, The complete light-curve sample of spectroscopically confirmed SNe Ia from Pan-STARRS1 and cosmological constraints from the Combined Pantheon Sample, Astrophys. J. **859**, 101 (2018).

[48] A. G. Riess, S. Casertano, W. Yuan, L. M. Macri, and D. Scolnic, Large magellanic cloud cepheid standards provide a 1% foundation for the determination of the Hubble constant and stronger evidence for physics beyond ΛCDM, Astrophys. J. **876**, 85 (2019).

[49] K. C. Wong *et al.*, H0LiCOW – XIII. A 2.4 per cent measurement of $H_0$ from lensed quasars: $5.3\sigma$ tension between early- and late-Universe probes, Mon. Not. R. Astron. Soc. **498**, 1420 (2020).

[50] M. J. Reid, J. A. Braatz, J. J. Condon, L. J. Greenhill, C. Henkel, and K. Y. Lo, The Megamaser Cosmology Project: I. VLBI observations of UGC 3789, Astrophys. J. **695**, 287 (2009).

[51] W. L. Freedman *et al.*, The Carnegie-Chicago Hubble Program. VIII. An independent determination of the Hubble constant based on the tip of the red giant branch, Astrophys. J. **882**, 34 (2019).

[52] C. Potter, J. B. Jensen, J. Blakeslee, P. Milne, P. M. Garnavich, and P. Brown, Calibrating the Type Ia supernova distance scale using surface brightness fluctuations, American Astronomical Society Meeting Abstracts 232, 319.02 (2018).

[53] C. D. Huang *et al.*, A near-infrared period–luminosity relation for Miras in NGC 4258, an anchor for a new distance ladder, Astrophys. J. **857**, 67 (2018).

[54] P. A. R. Ade *et al.* (Planck), Planck intermediate results - XXIV. Constraints on variations in fundamental constants, Astron. Astrophys. **580**, A22 (2015).

[55] L. Hart and J. Chluba, Updated fundamental constant constraints from Planck 2018 data and possible relations to the Hubble tension, Mon. Not. R. Astron. Soc. **493**, 3255 (2020).

[56] L. Hart and J. Chluba, New constraints on time-dependent variations of fundamental constants using Planck data, Mon. Not. R. Astron. Soc. **474**, 1850 (2018).

[57] A. G. Riess, S. Casertano, W. Yuan, J. Bradley Bowers, L. Macri, J. C. Zinn, and D. Scolnic, Cosmic distances calibrated to 1% precision with Gaia EDR3 parallaxes and Hubble Space Telescope photometry of 75 Milky Way Cepheids confirm tension with ΛCDM, Astrophys. J. Lett. **908**, L6 (2021).

[58] W. Skidmore *et al.* (TMT International Science Development Teams & TMT Science Advisory Committee), Thirty meter telescope detailed science case: 2015, Res. Astron. Astrophys. **15**, 1945 (2015).

[59] P. Behroozi *et al.*, The Universe at $z > 10$: predictions for *JWST* from the UNIVERSEMACHINE DR1, Mon. Not. R. Astron. Soc. **499**, 5702 (2020).